INELASTIC LATERAL BUCKLING OF STEEL BEAMS SUBJECTED TO REPEATED AND REVERSED LOADINGS *

by K. Takanashi I)
K. Udagawa II)
H. Tanaka III)

Synopsis

Repeatedly reversed loading tests at constant deflection amplitudes are conducted on the steel beams with H-shaped sections. The results of these tests show the quite different behaviors of the lateral buckling as compared with the behaviors under monotonically increasing loadings, which have been investigated by many researchers for the establishment of "plastic design" of steel structures. There existed the upper bound of deflection amplitude for each specimen, within which a stable hysteresis loop can be established and beyond which, however, the recorded force reduces in each cycle and hysteresis loop become unstable. It is worth to be noted that these critical deflection amplitudes are much lower in comparison with the case of static and monotonic loading tests.

Introduction

Many tall buildings are recently designed on the criterion that frame structures behave inelastically during severe earthquake. Hence, a nonlinear dynamic analysis is usually performed on the assumption that structural members are expected to show stable hysteresis loops in force-deformation relationships, but the failure due to buckling and deterioration of hysteresis curves are not taken into account. In inelastic or plastic range, steel structures often fail due to buckling because of the sudden reduction of rigidity and hence the studies on the lateral buckling of members under repeated loads must be required as well as other buckling problems.

Fig. 1 illustrates a typical mode of buckling for a simply supported beam under a monotonically increasing concentrated load and Fig. 2 shows the typical moment-rotation curve for plastically designed members, which are required that moment can reach the full-plastic moment,

---

* The outline of this paper were presented at 5th World Conference on Earthquake Engineering.

I) Associate Professor, II) Research Assistant, III) Professor, Institute of Industrial Science, University of Tokyo, Tokyo, Japan

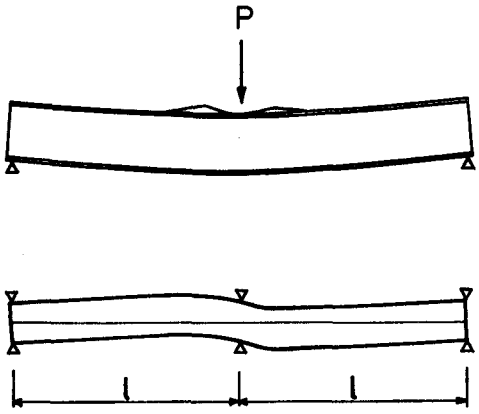

FIG. 1 LOCAL AND LATERAL BUCKLING

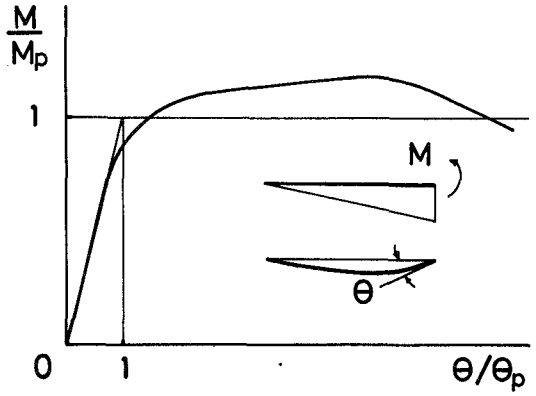

FIG. 2 MOMENT-ROTATION CURVE

M_p and a considerable amount of plastic deformation develops without moment reduction. The lateral buckling of a plastically designed beam occurs generally between lateral supports, and then the local buckling takes place in the compression flange near the loading point and, if the beam is designed by plastic method, the load continues to increase after buckling and the maximum moment is attained. To obtain the sufficient ductility of structures, the proportions of sections and spacing of lateral supports of members must be determined to possess much plastic deformation capacity.

The structural members subjected to severe earthquake are also considered to fail due to plastic buckling. Fig. 3 shows schematically the feasible deformation of a tall building which has stronger and more rigid columns than beams. Since "plastic hinges" develope in the ends of beams and rotate repeatedly and reversedly, buckling failure of beams must be investigated for reversed loads as well as monotonic loads.

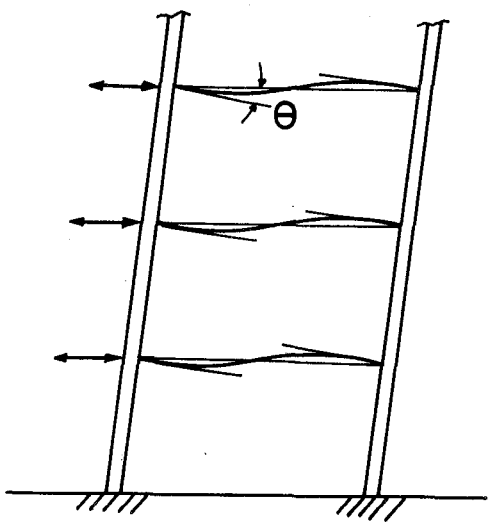

FIG. 3
DEFORMATIONS OF BEAMS IN A TALL BUILDING

Popov and Pinkney have carried out the cyclic bending tests on the cantilever steel beams and concluded that the load-deflection hysteresis loops keep remarkably stable shapes and the onset of local flange buckling does not imply an immediate loss of load carrying capacity, when closedly braced compact members are used.[1)2)] The beams in the real structures, however, cannot be always braced

closedly even though the attached slabs provide additional and uncertain restraints, so that this series of experiments is mainly intended to re-examine the provisions for lateral bracing requirements under repeatedly reversed loadings, which are recommended by AISC Specification, [3] AIJ Specification [4] etc. based on the plastic behaviors for the monotonically increasing loads.

Specimens and Test Set-up

Test specimens were fabricated from rolled H-shaped sections and are summarized in Table 1, where the unsupported length, the width-thickness ratio of flange, the depth-thickness ratio of web and the slenderness ratio with respect to weak axis for each specimen are shown. The unsupported lengths were determined so that the slenderness ratios vary from 50 to 80, because the specifications recommend 65 as the critical slenderness ratio. The specimens of DG series and DGH series

Table 1

	Geometric Properties				
	Section	l (cm)	B/t_f	H/t_w	l/r_y
DG-110-1	200x100x5.5x8	110	11.5	38.2	51.2
DG-110-2	"	"	11.7	38.1	51.3
DG-130-1	"	130	11.9	38.1	60.9
DG-130-4	"	"	13.3	37.4	62.5
DG-130-5	"	"	13.2	37.5	62.5
DG-150-2	"	150	11.6	38.1	70.0
DG-170-1	"	170	11.7	38.1	79.4
DG-170-3	"	"	13.2	37.4	81.7
DGH-110-1	200x100x5.5x8	110	12.3	37.1	52.2
DGH-110-2	"	"	12.2	36.4	52.3
DGH-130-1	"	130	12.5	35.7	62.2
DGH-130-2	"	"	12.4	36.9	61.9
DGH-150-1	"	150	12.4	35.8	72.0
DGH-150-2	"	"	12.4	36.4	71.6
DGH-170-1	"	170	12.5	37.4	80.7
DGH-170-2	"	"	12.5	36.8	80.9

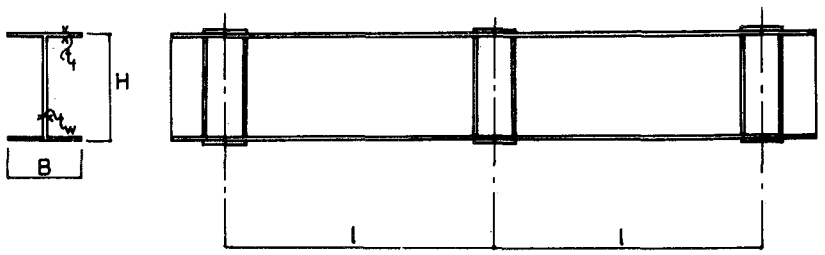

Table 2

Material Properties

Series		σ_y (t/cm^2)	σ_B (t/cm^2)	ε_y (x10^{-6})	ε_{st} (x10^{-6})	$\varepsilon_{st}/\varepsilon_y$	E_{st} (t/cm^2)	ε_B (%)
DG(1)	Flange	2.91	4.60	1390	16300	11.73	36.0	27.57
	Web	3.24	4.62	1540	22000	14.29	32.0	25.87
DG(2)	Flange	2.80	4.57	1330	17300	13.01	39.7	26.96
	Web	3.54	4.89	1690	23000	13.61	41.5	24.55
DGH	Flange	4.46	5.91	2120	16000	7.55	35.0	24.72
	Web	4.99	6.12	2380	27800	11.68	34.0	20.51

DG(1) : DG-110-1, DG-110-2, DG-130-1, DG-150-2, DG-170-1

DG(2) : DG-130-4, DG-130-5, DG-170-3

DGH : DGH-110-1, DGH-110-2, DGH-130-1, DGH-130-2, DGH-150-1
DGH-150-2, DGH-170-1, DGH-170-2

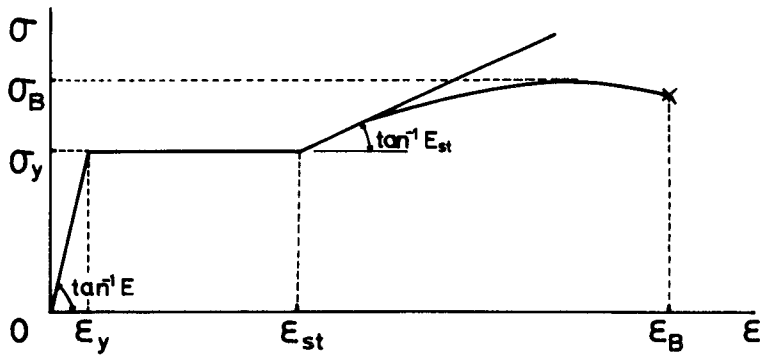

were made of JIS SS41 steel and JIS SM50 steel, respectively. The average yield stresses of flange and web are summarized in Table 2, which were evaluated by tension coupon tests. The full-plastic moment, M_p, of each beam was calculated for these values.

The rig employed to subject the beam specimens for reversed loadings is illustrated in Fig. 4 and Photo 1. Reversed loads were repeatedly applied by the hydraulic actuator at the center of the span, where a guide was provided to prevent lateral displacement and rotation with respect to beam axis, but not to prevent rotation with respect to strong and weak axes of beam section. At the both supported ends only lateral displacement and rotation with respect to beam axis were also prevented. This loading arrangement was intented to simulate the beam behaviors of a structure under lateral loads. In this simulation, however, some restraints provided by the torsional stiffness of columns were disregarded which restrain the beams to rotate with respect to weak axis at the ends of beams in real structures.

Photo - 1

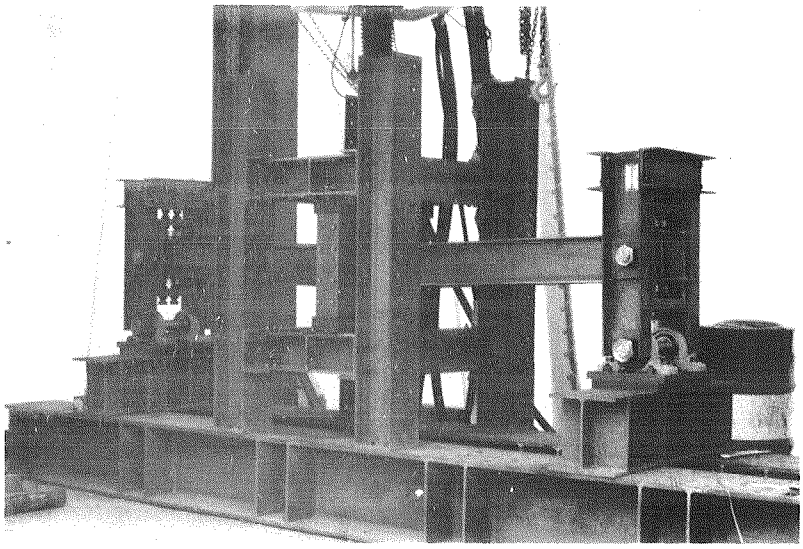

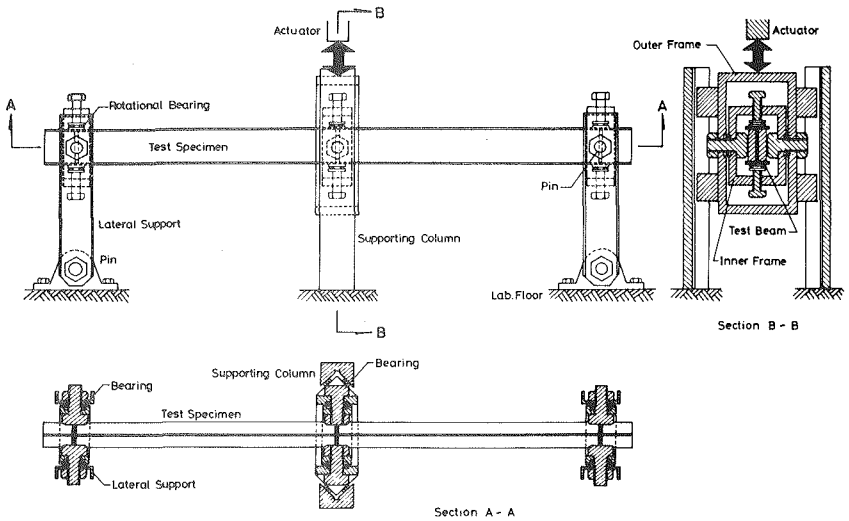

GENERAL VIEW OF TEST SETUP

FIG. 4 GENERAL VIEW OF TEST SETUP

The motion of the top of actuator was controlled by the servo controller. The displacement of the loading point was measured by a differential transformer type displacement transducer mounted there, and the output was fed back to the servo controller. The force applied to the beam was measured by the load cell interposed between the actuator's top and the loading point.

Test Procedure

A nearly half number of specimens were loaded statically and monotonically. These static test results and the previously obtained results by the authors are compared to the results of reversed loading tests.

The remaining specimens except DG-130-5 were repeatedly loaded at constant deflection amplitudes and loading sequences were summarized in Table 3. The amplitudes were increased to the next step in each 10

Table 3

SUMMARY OF TEST RESULTS

Specimen	Loading Condition	Frequency (Hz)	Cyclic Program θ/θ_p Ductility Ratio (Number of Cycles)	Rotation Capacity (R)
DG-110-1	Cyclic	0.03	1.0—2.0—2.5—3.0—3.5 (10) (〃) (〃) (〃) (15)	2.5
DG-110-2	〃	〃	1.0—1.5—2.0—2.5—3.0—3.5—4.0— (10) (〃) (〃) (〃) (〃) (〃) (〃) 4.5 (5)	2.0
DG-130-1	Monotonous	——		5.4
DG-130-4	Cyclic	0.03	1.0—2.0—2.5—3.0—3.5 (10) (〃) (〃) (〃) (〃)	2.0
DG-130-5	Earthquake Response[1]	0.067[2]	1.0—2.0—2.5—3.0—3.5—4.0—3.5— (1) (〃) (〃) (〃) (2) (〃) (1) 3.0[3] (1)	
DG-150-2	Cyclic	0.05	1.0—1.5—2.0—2.5—3.0—3.5 (10) (〃) (〃) (〃) (〃) (5)	1.7
DG-170-1	Monotonous	——		3.9
DG-170-3	Cyclic	0.03	1.0—1.5—2.0—2.5—2.75—3.0 (10) (〃) (〃) (40) (10) (5)	1.0
DGH-110-1	Monotonous	——		3.5
DGH-110-2	Cyclic	0.03	1.0—1.5—2.0 (10) (〃) (〃)	1.3
DGH-130-1	Monotonous	——		3.3
DGH-130-2	Cyclic	0.05	1.0—1.5—2.0—2.5—3.0 (10) (〃) (〃) (〃) (6)	1.1
DGH-150-1	Monotonous	——		2.4
DGH-150-2	Cyclic	0.05	1.0—1.5—2.0—2.5 (10) (〃) (〃) (〃)	1.0
DGH-170-1	Monotonous	——		1.5
DGH-170-2	Cyclic	0.03	1.0—1.5—2.0—2.5 (10) (〃) (〃) (3)	0.5

1) Response of deflection calculated with acceleration of ground motion recorded at Hachinohe 1968 earthquake

2) Mean frequency of response waves

3) Ratio of maximum response of rotation to θ_p

cycles in general. The cycle number of 10 in each step was considered to be sufficient to exclude the transient property of material after sudden change of loading.

The deflection was controlled so as to be sinusoidal function of time, t, in these tests. Of course, the displacement of real structures do not show the simple harmonic response during earthquake, but these tests results obtained for sinusoidal displacements were surely useful as a characteristic failure mode under cyclic loadings. As an attempt to evaluate the degree of failure by earthquake motion, DG-130-5 was loaded so as to trace the trajectory of a calculated deflection response in a simple structural model for an recorded earthquake.

The frequency of cyclic deflection was determined to be 0.03 or 0.05 Hz due to the capacity of the power supply, but this low frequency was convenient to measure force and deflection, and moreover, the validity of predicting dynamic behaviors by low frequency tests was already established by Hanson and Rea et al.[7]

Experimental Results

The end rotation, θ, and the end moment, M, defined by Fig. 5 were calculated from the central deflection and the applied force in each test. In order to compare the results in the same scale, θ and M are divided by θ_p and M_p, respectively.

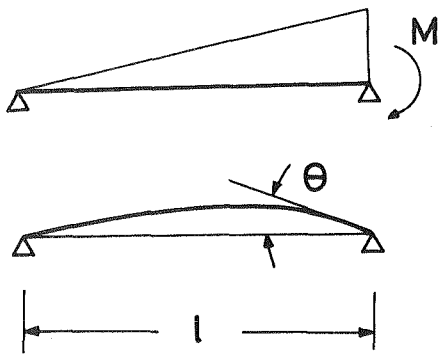

FIG. 5
DEFINITIONS OF MOMENT AND ROTATION

θ_p is given by the expression

$$\theta_p = M_p L/3EI_x \qquad (1)$$

where full-plastic moment, M_p, is calculated for the average yield stress in Table 2 and I_x is moment of inertia with respect to strong axis.

The moment-rotation relationships obtained by the monotonic loading tests are shown in Fig. 6, where the arrows indicate the maximum loads. According to the traditional way to express the rotation capacity often appeared in the papers on the plastic design, the rotation capacity, R, was calculated by

$$R = (\theta/\theta_p)_m - 1 \qquad (2)$$

In the monotonic loading tests, $(\theta/\theta_p)_m$ of the above expression was defined as the value of rotation, θ/θ_p, at the maximum moment. The rotation capacity, R, obtained for each specimen is summarized in Table 3 and plotted in Fig. 9 with the data previously obtained by the authors.

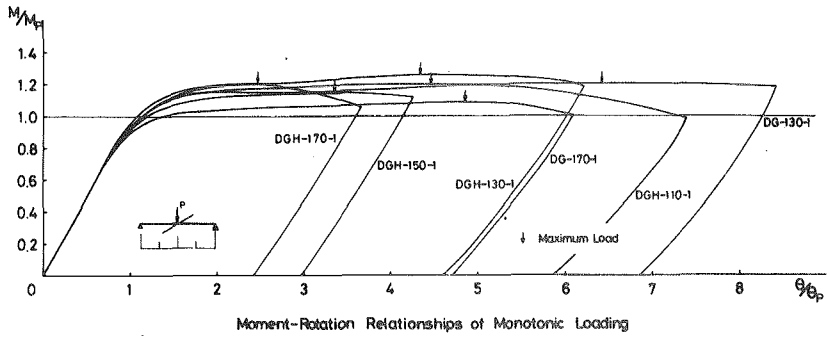

Moment-Rotation Relationships of Monotonic Loading

FIG. 6 MOMENT-ROTATION RELATIONSHIPS OF MONOTONIC LOADING

When a beam was monotonically loaded further beyond the peak of M/M_p-θ/θ_p curve, the lateral buckling deformation of a beam developed remarkably and consequently the magnitude M/M_p decreased. After that, for reversed loads no stable hysteresis loop could be obtained.

In the case of reversed bending tests the moment-rotation hysteresis curves were obtained as shown Figs. 7 and 8, where inserted numerals beside loops denote the numbers of cycles. These curves were calculated from the load-deflection hysteresis curves recorded by x-y plotter. As recognized by the figures, the hysteresis loops could keep their very stable shapes as long as the amplitude was controlled within some critical bound. Once the amplitude exceeded the critical bound, lateral buckling was accelerated, the hysteresis loops become unstable and the magnitude of M/M_p decreased in each cycle. In general the permanent lateral displacements of flange plates are caused by plastic buckling and cannot recover to the initial positions. As the lateral displacement of upper and lower flanges were alternatively accumulated by reversed bending, it seems as if the beams had been bent laterally after load was removed. The buckled deformation of flange near loading point is illustrated in Photo 2.

The failure due to lateral buckling is defined in this series of experiments as follows: After 10 cycles at the same amplitude the moment reduces more than 5% of the first attained value and moreover the rate of reduction asymptotically vanishes.

The critical amplitude is defined as the amplitude, beyond

Photo 2

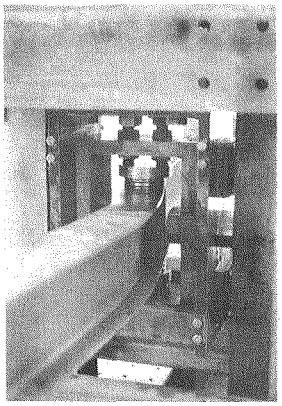

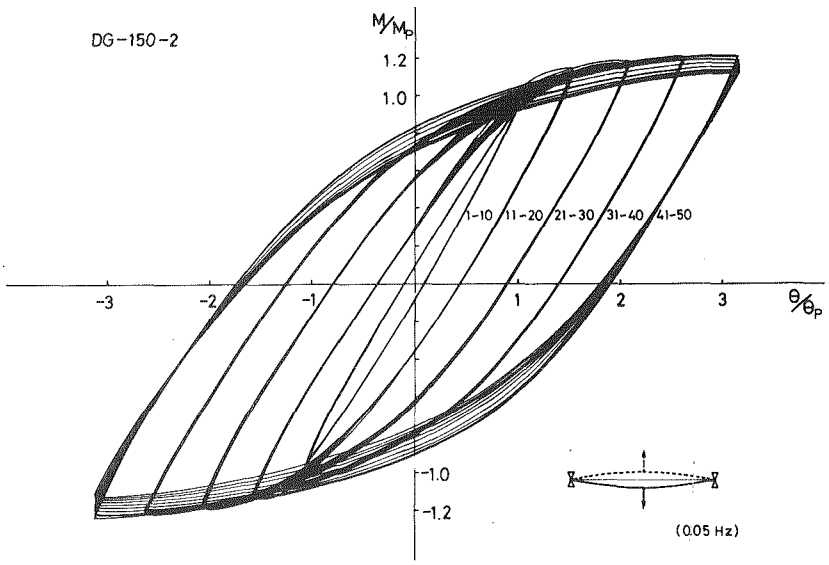

FIG. 7 HYSTERESIS LOOPS

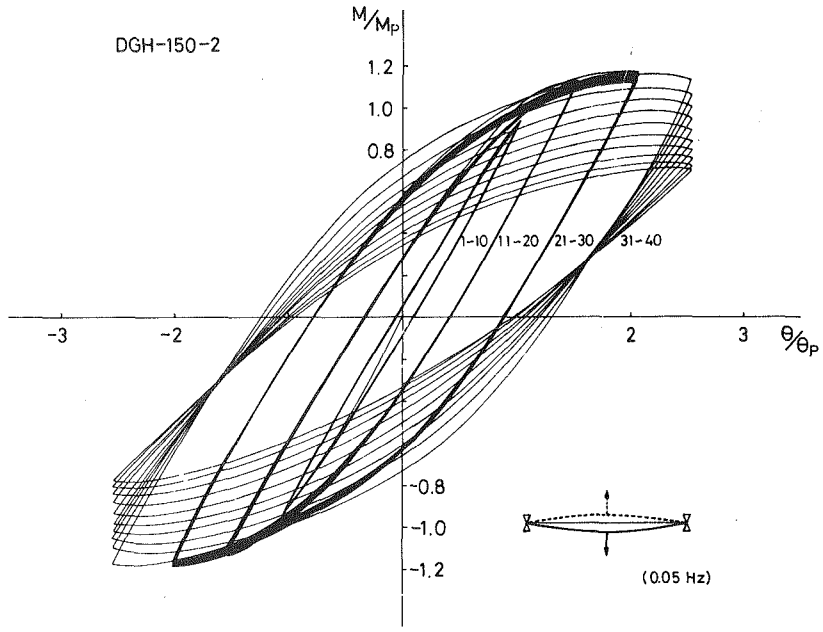

FIG. 8 HYSTERESIS LOOPS

which beam fails, and denoted by $(\theta/\theta_p)_m$ to compare with results of the monotonic loading tests. R is defined by Eq. (2).

The rotation capacity, R, obtained for all specimens are plotted in Fig. 9 as a function of slenderness ratio, L/r_y, where L is the unsupported length. In Fig. 9 the open circles represent the results of DG series and the open triangles the results of DGH series for monotonic loading tests. On the other hand the solid circles and triangles indicate the results of DG series and DGH series for reversed loading tests, respectively. The solid curve in the figure is a regression curve which was made to be fitted on a Log-Log paper. It can be seen that R for the reversed loads are considerably lower than for the monotonic loads.

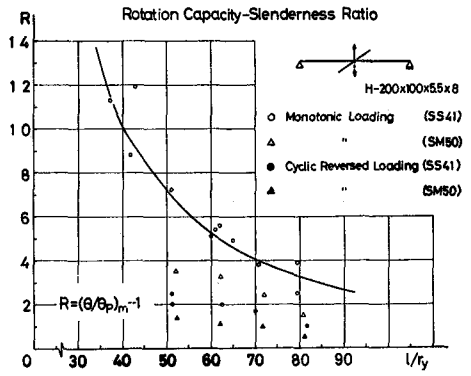

FIG. 9
ROTATION CAPACITY-SLENDERNESS RATIO

Only a specimen, DG-130-5, was loaded so as to follow the calculated deflection response of a simple structural model. This is a trial for grasping what kind of hysteresis loops and what state of lateral buckling real members show when structures are subjected to severe earthquakes. For comparison of the above results with the results of a sinusoidal loading test the recorded deflections, δ, and forces, P, for DG-130-4 and DG-130-5, which have the same geometric properties, are shown in Fig. 10. The height of the maximum peak of deflection curve for DG-130-5 is set to $3.5\theta/\theta_p$ and the amplitude of the sinusoidal curve of deflection for DG-130-4 is the same value of $3.5\theta/\theta_p$. The hysteresis loops for DG-130-5 are shown in Fig. 11, where Fig. 11(a) is the loops for the first loading due to the calculated deflection shown as Fig. 10 and Fig. 11(b) is the loops for the second loading due to the same deflection curve. By these figures, a little reduction of moment, M/M_p, is recognized but it is not so much as the reduction for DG-130-4 at the amplitude of $3.5\theta/\theta_p$. In fact the reduction of moment for the sinusoidal loading is remarkable when the amplitude is beyond the critical. For example, the hysteresis loops of $3.0\theta/\theta_p$ and $3.5\theta/\theta_p$ for DG-130-4 are displayed in Fig. 12, where the critical amplitude is determined to be $3.0\theta/\theta_p$ according to the previously mentioned difinition.

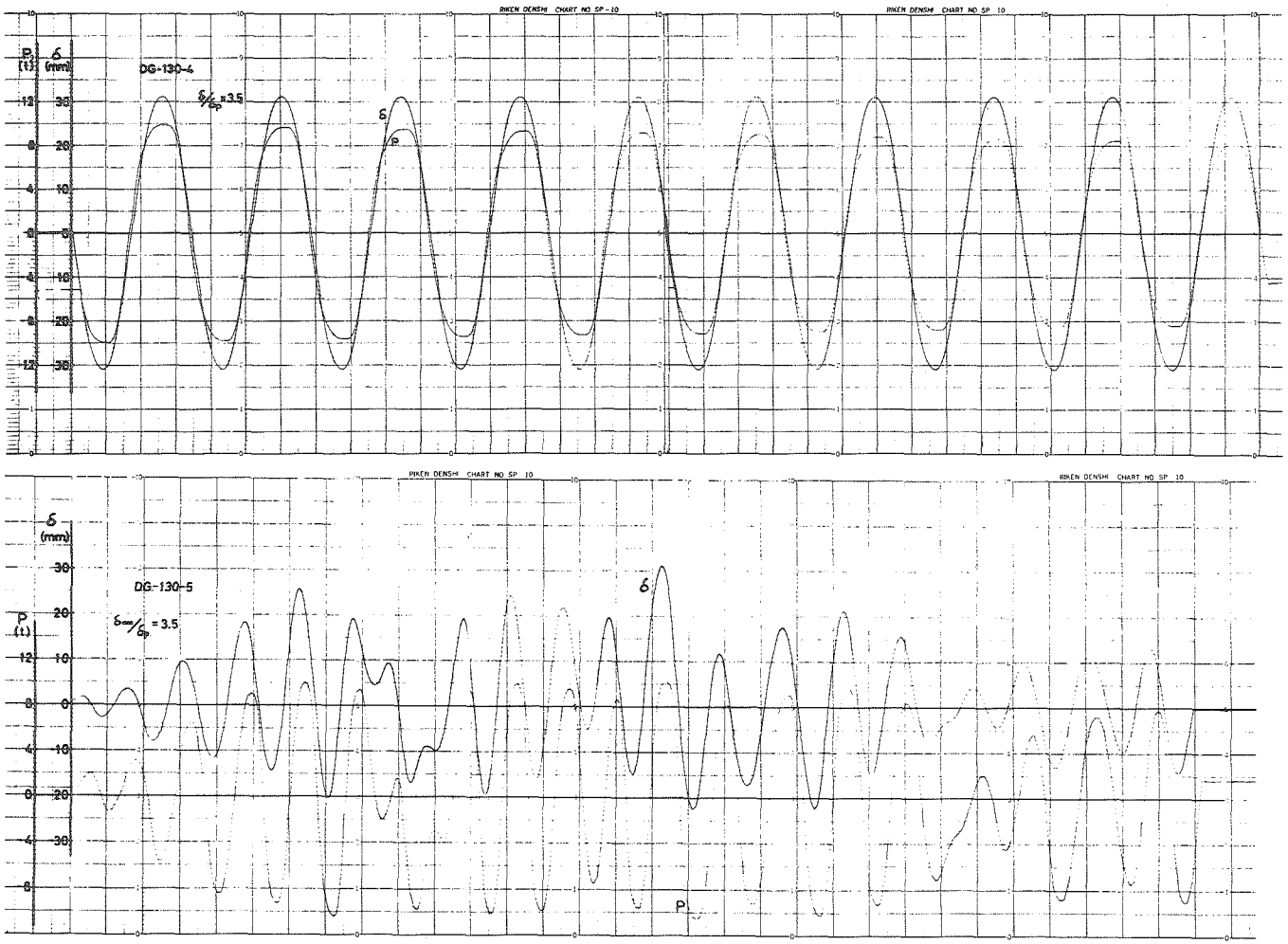

FIG. 10 APPLIED DEFLECTIONS AND FORCES

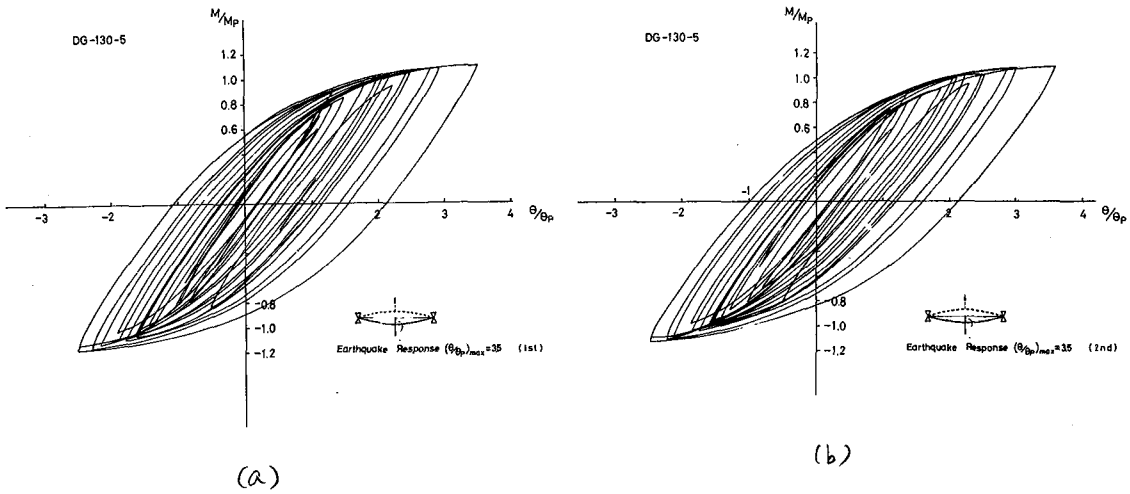

(a) (b)

FIG. 11 HYSTERESIS LOOPS

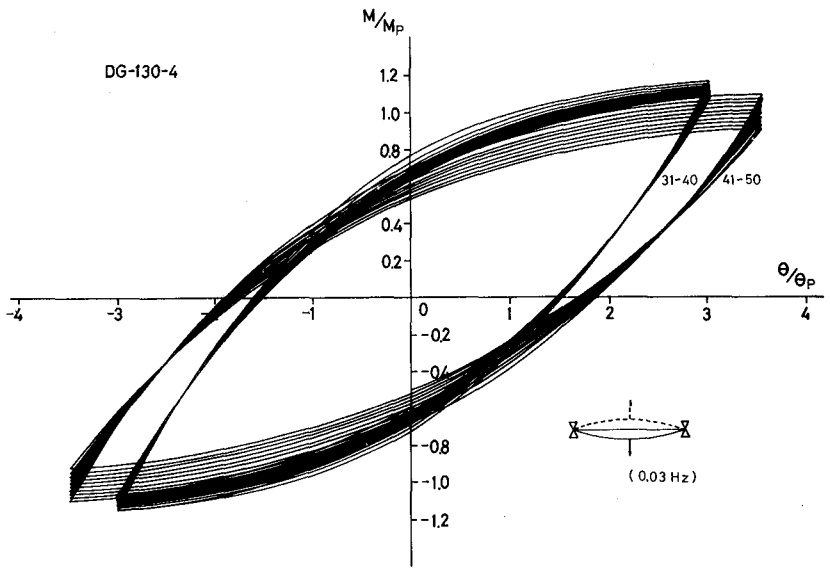

FIG. 12 HYSTERESIS LOOPS

Conclusions

From the above discussions, the following are concluded.

1) For repeated loading, stable moment-rotation hysteresis loops can not be obtained after severe lateral buckling occurred by monotonically increasing loads.
2) There exists the critical amplitude of deflection, within which the hysteresis loops are stable under repeated loads and beyond which the load carrying capacity of the beam reduces in each cycle.
3) These critical amplitudes are considerably low in comparison with the deflections at the maximum loads in the monotonic loading tests. It is worth to be noted that the critical values for cyclically reversed loadings are lower than a half of the critical values for monotonic loadings.
4) For SM50 steel, more severe bracing requirements for lateral buckling must be provided to beams of structures subjected to both monotonic and cyclically repeated loads.
5) The degree of failure due to lateral buckling for the test so as to follow the response to earthquake are not same as that of failure by the cyclic test at a constant amplitude even though the maximum deflections were adjusted to be equal.

Acknowledgements

The authors wish to express their gratitude to Associate Professor T. Okada for affording his calculation results of response.

Assistants T. Shigenobu and Y. Shimawaki are also much appreciated for their valuable assistance during this series of experiments.

References

1) V. V. Bertero and E. P. Popov, "Effect of Large Alternating Strains of Steel Beams," Proc. ASCE, ST 1, Feb. 1965
2) E. P. Popov and R. B. Pinkney, "Cyclic Yield Reversal in Steel Building Connections," Proc. ASCE, ST 3, March 1969
3) "AISC Specification for the Design, Fabrication and Erection of Structual Steel for Buildings," Feb. 1969, American Institute of Steel Construction
4) "AIJ Specifications for Plastic Design of Steel Structures (Draft)," 1971, Architectural Institute of Japan
5) R. D. Hanson, "Comparison of Static and Dynamic Hysteresis Curves," Proc. ASCE, EM 5, Oct. 1966
6) P. D. Hanson, A. M. AlMuti and J. G. Hoad, "Post-Elastic Response of Mild Steel Structures," Proc. 3rd. Japan Earthquake Eng. Sym. 1970
7) D. Rea, R. W. Clough, J. G. Bouwkamp and U. Vogel, "Damping Capacity of a Model Structure," Proc. 4th World Conf. Earthquake Eng. 1969